Renewable and Sustainable Energy Reviews 31 (2014) 149–157

Contents lists available at ScienceDirect

Renewable and Sustainable Energy Reviews

journal homepage: www.elsevier.com/locate/rser

Electron transport analysis in zinc oxide-based dye-sensitized solar cells: A review

Azimah Omar, Huda Abdullah *

Department of Electrical, Electronic and System Engineering, Faculty of Engineering and Built Environment, Universiti Kebangsaan Malaysia, 43600 Bangi, Selangor, Malaysia

ARTICLE INFO

Article history:
Received 4 April 2012
Received in revised form
11 October 2013
Accepted 18 November 2013
Available online 12 December 2013

Keywords:
ZnO
Dye-sensitized solar cell
Nanostructures
Impedance
Electron transport

ABSTRACT

This research review highlights the use of zinc oxide (ZnO) nanostructure as a photoanode in the fabrication of dye-sensitised solar cells (DSSC). ZnO nanostructure thin films offer large surface area, direct electron pathways and effective light scattering centre. The fabrication work can produce a variety of ZnO nanostructures, from nanotubes, nanoporous, nanosheets, nanoflowers, nanoflakes, nano-branches and nanolipsticks. The internal mechanism inside the cell gives useful information on the electron transport properties and efficiency of ZnO-based DSSC. The review ends with an outlook highlighting the electron transport parameters analysed by electrochemical impedance spectroscopy (EIS) unit. Such parameters including charge transport resistance (R_{ct}), transport resistance (R_t), chemical capacitance (C_μ), effective electron lifetime (τ_{eff}), effective electron chemical diffusion coefficient (D_{eff}), effective rate constant for recombination (k_{eff}), effective electron diffusion length of the photoanode (L_n) and finite Warburg impedance in the electrolyte (Z_D). Monitoring the electron transport properties may improve the photovoltaic performances of the ZnO-based DSSC such as open circuit voltage (V_{oc}), short circuit current density (J_{sc}), fill factor (FF) and power conversion efficiency (η).

Contents

1. Introduction

Sunlight provides a clean, renewable and cheap energy source for people, while also serving as a primary energy source for another type of energy resources, such as water, bio-energy, wind energy and fossil fuel. However, the use of fossil fuels has contributed to the recent increase in the greenhouse gas effect and CO_2 emissions, as well as global warming. One way to overcome these issues is by introducing several types of renewable energy. The most abundant renewable energy source is solar radiation, which provides very high temperature heat that can power up a mechanical engine by converting the radiation into a mechanical power and electricity to drive a generator or a machine. Solar power can also be directly converted into electricity unit by a photovoltaic (PV) effect. Single-junction crystal solar cells or single and multi-crystalline silicon solar cells are the first generation of PVs technology. Second-generation PV technologies introduced a thin film to reduce the material cost. The current third-generation PV technologies incorporate double junctions, triple junctions and nanotechnology into solar cell fabrication methods [1]. One example of these third-generation technologies is dye-sensitized solar cell (DSSC), which provides a low cost

* Corresponding author. Tel.: +603 89216310; fax: +603 89216146.
E-mail addresses: huda@vlsi.eng.ukm.my, huda@eng.ukm.my (H. Abdullah).

1364-0321/$ - see front matter
http://dx.doi.org/10.1016/j.rser.2013.11.031

method to convert sunlight to electricity. It is also known as a photoelectrochemical cell or photoactive electrode based on a nanostructured metal-oxide film, such as TiO_2, ZnO, SnO_2, Nb_2O_5, $SrTiO_3$, CdSe, CdS, Fe_2O_3, WO_3 and Ta_2O_5 [2–5].

DSSC was firstly introduced by O'Regan and Grätzel in 1991 by implementing a TiO_2 nanocrystalline material as photoanode or photoelectrode [2]. In general, DSSC consist of five main components: (1) a glass substrate of transparent conductive oxides (TCO); (2) a mesoporous semiconductor metal-oxide layer; (3) a monolayer of organic dye molecules attached to the surface of the nanocrystalline film; (4) a liquid electrolyte containing a redox couple iodide/traded that interpenetrates the dye-coated nanoparticles and (5) a platinum counter electrode [6–8]. The working principle of DSSC was reported as different from a conventional solar cell, where the light absorption and carrier transportation inside the cell occurs separately [6]. An exciton is split into an electron and a hole due to the absorption of light. The light is absorbed by a ruthenium complexes dye, such as [Ru(4,4′-dicarboxy-2,2′-bipyridine ligand)$_3$] or N719 [8] that is attached to the photoanode via a carboxylate element. The TiO_2 semiconductor oxide layer with 10–20 nm diameter nanocrystals are deposited on a TCO substrate and annealed at high temperature to form a ~16 μm thick film [9]. As shown in Fig. 1, the absorption of a photon by the sensitized/dye, S occurred inside the cell (Eq. (1)). Consequently, within femtoseconds, the excited electrons are elevated from a molecular ground state, S, to an excited state, S^* (Eq. (1)). The excited electron is then injected into the conduction band (CB) of the semiconductor layer, leaved the dye molecule in an oxidized state, S^+ (Eq. (2)). The electrons disperse into the porous semiconductor layer, move to the TCO glass layer and external load via a counter electrode (CE). At the counter electrode, a redox mediator is reduced to iodide (I^-) due to the electron transfer in the electrolyte layer (Eq. (3)). The sensitizer will be regeneration by the iodide ions which may interrupt the recapture of electron by the oxidized dye (Eq. (4)). However, a recombination may occur between the injected electrons either with the oxidized dye (Eq. (5)) or with the oxidized redox couple at the photoanode surface area (Eq. (6)) [8,10–12]. The mechanisms can be summarized as a complete photovoltaic energy conversion equation [8]:

$$S_{(adsorbed)} + h\nu \rightarrow S^*_{(adsorbed)} \quad (1)$$

$$S^*_{(adsorbed)} \rightarrow S^+_{(adsorbed)} + e^-_{(injected)} \quad (2)$$

$$I_3^- + 2.e^-_{(cathode)} \rightarrow 3I^-_{(cathode)} \quad (3)$$

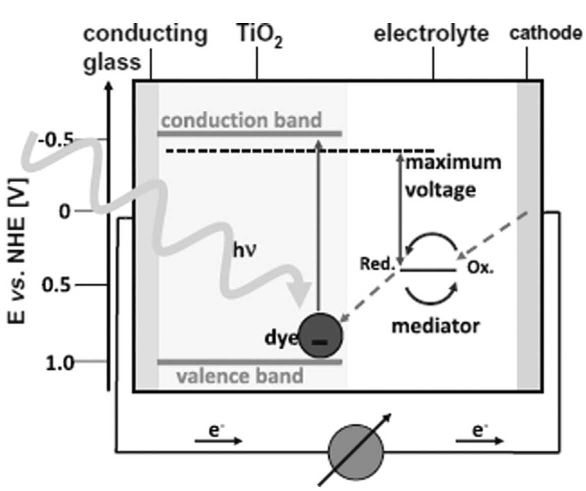


Fig. 1. Principle operation and energy level scheme of the dye-sensitized solar cell [8].

$$S^+_{(adsorbed)} + \frac{3}{2}I^- \rightarrow S_{(adsorbed)} + \frac{1}{2}I_3^- \quad (4)$$

$$S^+_{(adsorbed)} + e^-_{(TiO_2)} \rightarrow S_{(adsorbed)} \quad (5)$$

$$I_3^- + 2 \times e^-_{(TiO_2)} \rightarrow 3I^-_{(anode)} \quad (6)$$

Since the performance of solar cells is measured based upon their power conversion efficiency, dye-sensitized solar cells (DSSCs) are expected to generate high efficiency at low production cost compare to the conventional single-crystal silicon-based. The most successful DSSC based on TiO_2 photoanode combined with a "black dye" tri(cyanato)-2,2′2″-terpyridyl-4,4′4″-tricarboxylate)Ru (II) achieved greater efficiency of 10.4% (1.5 AM) [6]. This figure then improved to 11.4% in 2012 as achieved by Han et al. [13]. Currently, the efficiency has increased to 15% by fabricating a perovskite pigment within a nanoporous TiO_2. The implementation of perovskite was reported as a main reason that improved the TiO_2-based DSSC [14]. Previous researchers have also reported other factors that influenced the solar cell's performance. Lee et al. mentioned implementing a wide band gap metal oxide semiconductors as a photoanode increases the cell's surface area, light absorption and dye loading [2]. Furthermore, efficiency and stability of the solar cells can be investigated from the kinetic parameters of the charge transfer. Moreover, Goncalves et al. reported that the efficiency can be increased by reducing the number of electrons that recombine with the oxidized species from the redox system, monitoring the energy mismatches between the dye and the redox species and increasing the electron diffusion throughout the semiconductor porous nanostructure layer [15]. Consequently, from our point of view, understanding the cell's internal mechanism is important to analyze the electron transport, diffusion, recombination and generation between the photoanode, semi-conductor layer/dye/electrolyte, and counter electrode. This analysis can be conducted by developing a transmission line equivalent circuit model consisting of resistance, capacitance and impedance components by using an electrochemical impedance spectroscopy (EIS) unit [16]. A fitting process of the equivalent circuit is required to measure and analyze the respective electron transport parameters such as charge transport resistance (R_{ct}), transport resistance (R_t), chemical capacitance (C_μ), effective electron lifetime (τ_{eff}), effective electron chemical diffusion coefficient (D_{eff}), effective rate constant for recombination (k_{eff}), effective electron diffusion length of the photoanode (L_n) and finite Warburg impedance in the electrolyte (Z_D). Consequently, we can monitor the photovoltaic performances of the DSSCs including open circuit voltage (V_{oc}), short circuit current density (J_{sc}), fill factor (FF) and power conversion efficiency (η) [15–25]. Andrade et al. mentioned that the current–voltage ($I-V$) curve estimations and electron transport analysis provide a deeper understanding of the internal mechanisms of the DSSC [26]. In this review, we would like to highlight the electron transport properties in the ZnO-based DSSCs which is quite similar to the TiO_2-based DSSC. Thus, ZnO needs to have similar photoelectrode properties and equivalent electron affinity as TiO_2 metal oxide material to improve the light harvesting efficiency and electron injection mechanism inside the cell.

2. Zinc oxide as a photoanode

ZnO has been used as a pigment, a protective coating on metal surfaces and as a UV-absorbing additive for sunscreen protection, cosmetic products [27], plastics and rubber composites [28]. Recently, ZnO has also been widely used in high technology applications such as in short wavelength opto-electronic devices, photonic crystals, photodetectors, photodiodes, photovoltaic, gas

sensors, dye-sensitized solar cells, gas sensors [4], light-emitting diodes, optical devices [29], photocatalyst [30], surface acoustic wave devices [31], UV detectors, field emissions, biosensors, photoluminescent materials, anti-bacterial purposes [32] and piezoelectric devices [33–36]. Prior to Grätzel's implementation of the first TiO_2-based DSSCs in 1991, Gerischer and Tributsch have proposed ZnO as an effective choice of photoanode [3]. ZnO with wide bandgap energy similar to TiO_2 ($E_g \approx 3.37$ eV) [37] and higher electron mobility compared to TiO_2 may overcome higher electron recombination in the TiO_2-based DSSCs [38,39]. Such recombination occurs due to very fast electron injection (femto seconds) from a photoexcited dye into the conduction band of TiO_2. Although, the efficiencies of ZnO are still far behind that of TiO_2 (lower than 8%) [40], a few studies have been highlighted by researchers in this field to improve the power conversion efficiency of ZnO-based DSSC. Martinson found that ZnO's surface morphologies were more amenable to modification compared to those of TiO_2, which can increase the overall power conversion efficiency by increasing the dye loading capacity and decreasing the recombination effect inside the cell [41]. For example, Liu et al. fabricated a variety of ZnO nanostructures, including nanoparticles, ordered porous, nanorods, nanotubes and porous nanosheets [42] to improve the light harvesting, electron transport and power conversion efficiency of the cells. Other researchers developed other structures such as nanowires [4], nanoflakes [43], nanobelts [44], nanoflowers [4,45], nanocombs [46], nanoclusters, nanocolloids, nanopowders and self-assembled nanomaterials [47]. ZnO nanowires and nanotubes provide a unidirectional conduction path for rapid electron transport inside photoanode films [48]. The branched ZnO nanowires improved the overall efficiency of the solar cell from 0.75% (bare ZnO nanowires) to 1.51%. The branched wires' direct conduction pathway and higher dye absorption significantly influenced their performance. Fig. 2 shows low and high magnification images of the branched ZnO nanowires [48].

Moreover, ZnO photoanode has great ability to be synthesized at low temperature level with the simple fabrication work of chemical bath deposition [49], sol–gel [50], sputtering or electrodeposition [28] method. In general, increasing the temperature from 20 °C to 60 °C or to a normal state did not prompt the temperature or power conversion efficiency differences. Instead, the DSSC became less sensitive to the light incidence angle compared with Si-based solar cells [28]. Besides that, ZnO nanorods can be fabricated at low deposition times as reported by Hossain et al. A structure similar to lipsticks appeared in the photoanode surface area. However, the growth of the nanolipsticks structures decreased at a longer deposition time. At the final stage of their experimental work, the substrate area was fully transformed into nanorods structures [51]. On the other hand, Keis et al. mentioned that similar electron transport properties of ZnO with TiO_2 increases its ability to harvest light and becomes as efficient as TiO_2-based DSSCs [52]. It has then become our main interest in this recent review to introduce the electron transport analysis inside the ZnO-based DSSC.

3. Electron transport analysis inside the DSSC

Basic knowledge of electron transfer, internal electrical characteristic and kinetic movement of the active particles inside the ZnO-based DSSC suggests that they are as effective as TiO_2 photoanode [53]. Fig. 3 shows a state diagram of the kinetic information of electron transfer, charge transport processes (blue arrows) and loss reactions (grey arrows) [54]. The electron injection time from the excited dye to the conduction band should exceed the excited state decay to the ground within femtosecond to picosecond [54,55]. Gratzel et al. reported the electron injection rates is very much dependent on the electronic coupling between the dye excited-state LUMO orbital and accepting states in the photoanode, and relative energies of the state [54]. In addition, Ahmed mentioned that the injection rate depends on the particle connectivity and morphologies of the thin film [55]. In general, fast electron injection dynamics require a strong electronic coupling of the dye LUMO orbital to the metal oxide CB states and sufficient free energy difference. Moreover, dye regeneration requires the rate of re-reduction exceed the charge recombination of injected electrons (within 1 ms). Efficient charge transport to the counter electrode/external circuit then takes up within millisecond to second. Faster time constant than charge recombination is expected due to electron trapping in the sub-bandgap states. Consequently, the main loss mechanisms in the state-of-the-art

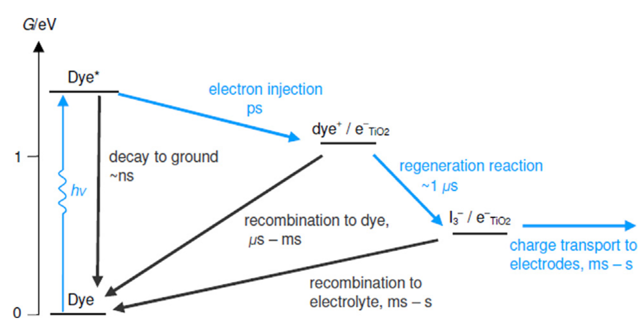


Fig. 3. State diagram representation of the kinetics of DSSC. Forward processes of light absorption, electron injection, dye regeneration and charge transport are indicated by blue arrows. The competing loss pathways of excited-state decay to ground and electron recombination with dye cations and oxidized redox couple are shown in grey arrows [54]. (For interpretation of the references to color in this figure legend, the reader is referred to the web version of this article.)

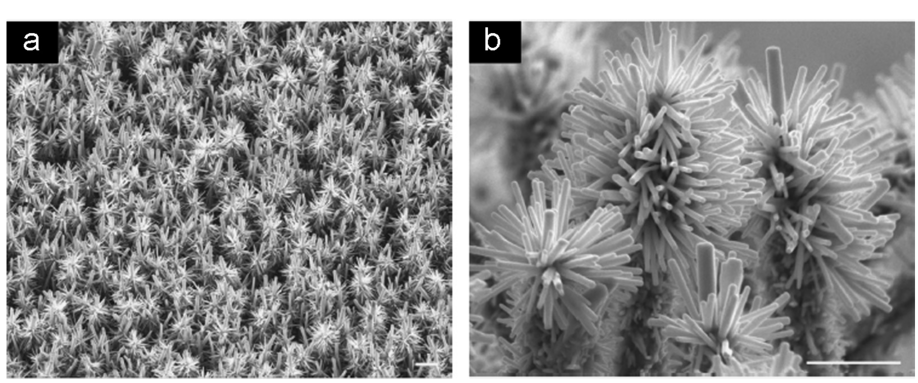


Fig. 2. (a) Low- and, (b) high-magnification FESEM images of the branched ZnO nanowires after second growth; scale bar, 1 μm [48].

DSSC device include decay of the dye excited state to ground and charge recombination of injected electrons with dye cations and with the redox couple. The charge recombination with the dye cations occur within a time scale of microsecond to millisecond faster than the recombination with the electrolyte (millisecond to second) [54]. Martinson reported the kinetic process of electron in the DSSC is sensitive to excitation wavelength and dye-loading conditions. The situations can be prevented by simultaneously accelerating back electron transfer from the photoanode to the dye or speeding up the charge transport to the external circuit [41]. Thus, the kinetic competition between the charge transport and recombination has been analyzed in terms of photoanode thickness, L and its effective electron diffusion length, L_n [41,56]:

$$L_n = \sqrt{D_{eff}\tau_{eff}} \tag{7}$$

where D_{eff} is the effective diffusion coefficient for the electron within the photoanode and τ_{eff} is the effective electron lifetime due to charge recombination with the oxidized dye. L_n should be greater than L in order to absorb more incident light. The result is high light harvesting efficiency (LHE), good charge collection efficiency (η_c) and both of them influence the increment of incident photon-to-current efficiency (IPCE) [41]:

$$IPCE = LHE \times \Phi_{inj} \times \eta_c \tag{8}$$

where Φ_{inj} is the efficiency of electron injection from the excited dye into the semiconductor framework. Therefore, faster electron transport is expected where it increases the amount of photocurrent-density, J_{sc}. In the most efficient liquid electrolyte, L_n is already greater (at most wavelengths) than L to collect most of the incident photons. Therefore, faster electron transport (larger D_{eff}) is impossible for faster interception (shorter τ_n). Furthermore, the values of L_n, D_{eff}, τ_{eff} and other electron transport parameters can further be analyzed from the impedance spectra and equivalent circuit model of the DSSC.

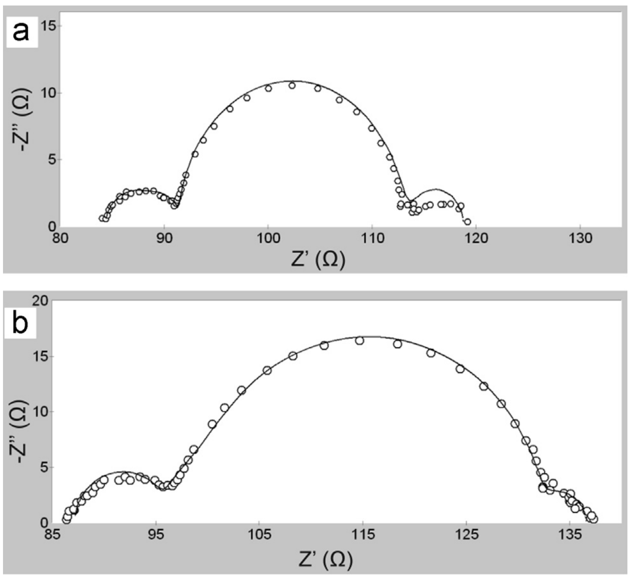


Fig. 4. Impedance spectra of ZnO-based DSSC analyzed by EIS unit [20].

4. Impedance spectra analysis and equivalent circuit model

Generally, impedance spectra of the DSSCs is recorded under one sun (AM 1.5) light intensity. Fig. 4 shows the example of impedance spectra of ZnO-based DSSC measured by EIS unit. The spectra cover three main regions; high frequency region (1 kHz to

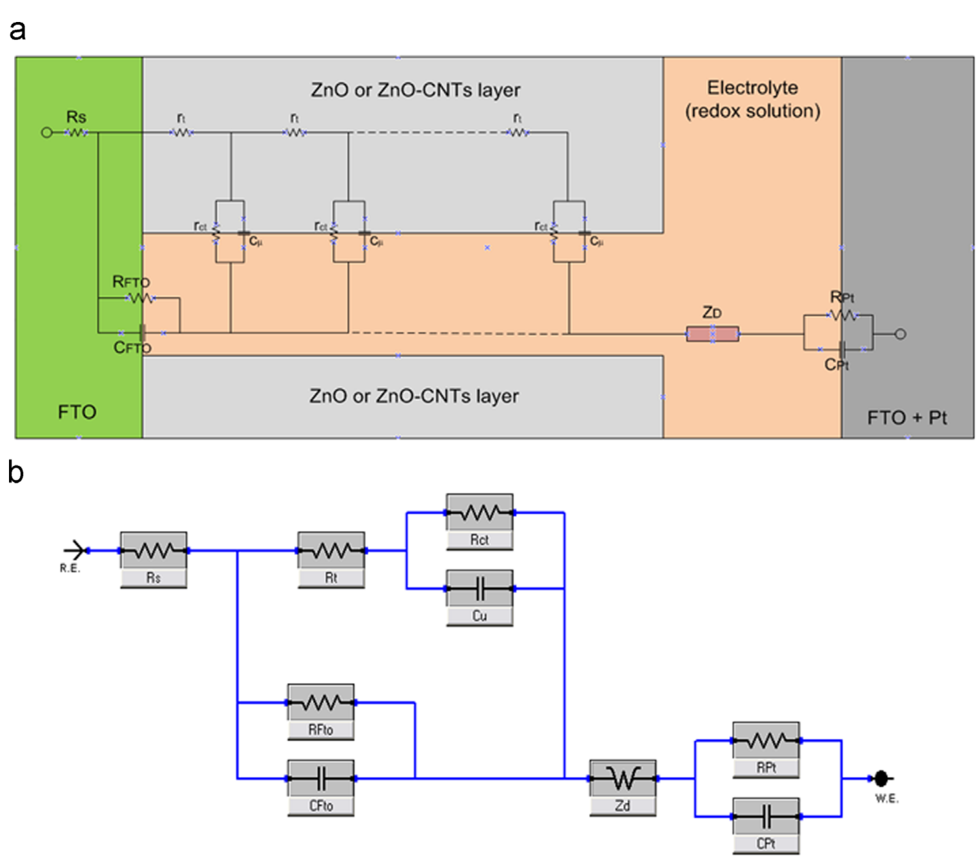


Fig. 5. (a) Transmission line equivalent circuit model and (b) equivalent circuit model for fitting process in the GAMRY Model Editor [39].

Table 1
Photovoltaic and electron transport properties of ZnO-based DSSC determined by electrochemical impedance spectroscopy.

ZnO-DSSC	Photovoltaic properties				Electron transport properties												Reference
	J_{sc} (mA/cm^2)	V_{oc} (V)	FF	η (%)	L (μm)	ω_{max} (Hz)	R_s (Ω)	R_{ct} (Ω)	R_t (Ω)	R_{Pt} (Ω)	C_μ (μF)	Z_D	τ_{eff} (ms)	k_{eff} (s^{-1})	D_{eff} (cm^2 s^{-1})	L_n (μm)	
Bare NWs	2.37	0.636	0.498	0.75	–	–	–	92.12	3.63	–	–	–	26	38.31	6.23e-4	–	Cheng et al. [48]
Branched NWs	4.27	0.675	0.522	1.51	–	–	–	86.85	3.36	–	–	–	38	26.31	4.35e-4	–	Cheng et al. [48]
Nanocombs	3.14	0.671	0.34	0.68	–	–	213	29.6	–	–	–	–	–	–	–	–	Umar, [46]
Tetrapod	12.3	0.6	0.65	4.9	42.2	–	–	11.06	9.48	–	–	–	13.54	–	1.533e-3	45.57	Chiu et al. [37]
Short-tetrapod	10.79	0.66	0.67	4.78	26	28.36	–	18.95	1.36	–	–	–	35.26	28.36	2.47e-3	93.32	Lee et al. [60]
Long-tetrapod	8.59	0.63	0.65	3.52	36	108.70	–	15.04	2.21	–	–	–	9.20	108.70	4.62e-3	65.20	Lee et al. [60]
ZnO	–	–	0.41	–	–	–	–	200-10e^4	67–100	6.79	–	–	–	–	–	–	He et al. [59]
Nanoflakes	6.732	0.533	0.505	1.81	–	–	–	3.794	1.135	–	–	–	6.36	–	1.7e-3	32.9	Ariyanto et al. [20]
NRs	4.14	0.48	0.45	0.90	–	28.2	–	373.9	–	–	–	–	2.93	–	–	–	Lin et al. [61]
NPs	6.50	0.56	0.50	1.80	–	–	–	101.8	–	–	–	–	0.64	–	–	–	Lin et al. [61]
NRs/NPs	7.00	0.60	0.52	2.19	–	–	–	61.20	–	–	–	–	1.71	–	–	–	Lin et al. [61]
ZnO	3.3	0.739	0.64	1.6	64	–	–	–	–	–	–	–	–	–	0.4	–	Martinson et al. [23]
ZnO	1.78	0.22	0.64	0.25	2.74	600	50.48	31.55	118	4.68	7.099	2.542e^{-3}	0.266	3760	0.0755e^{-3}	0.0201	Omar et al. [39]

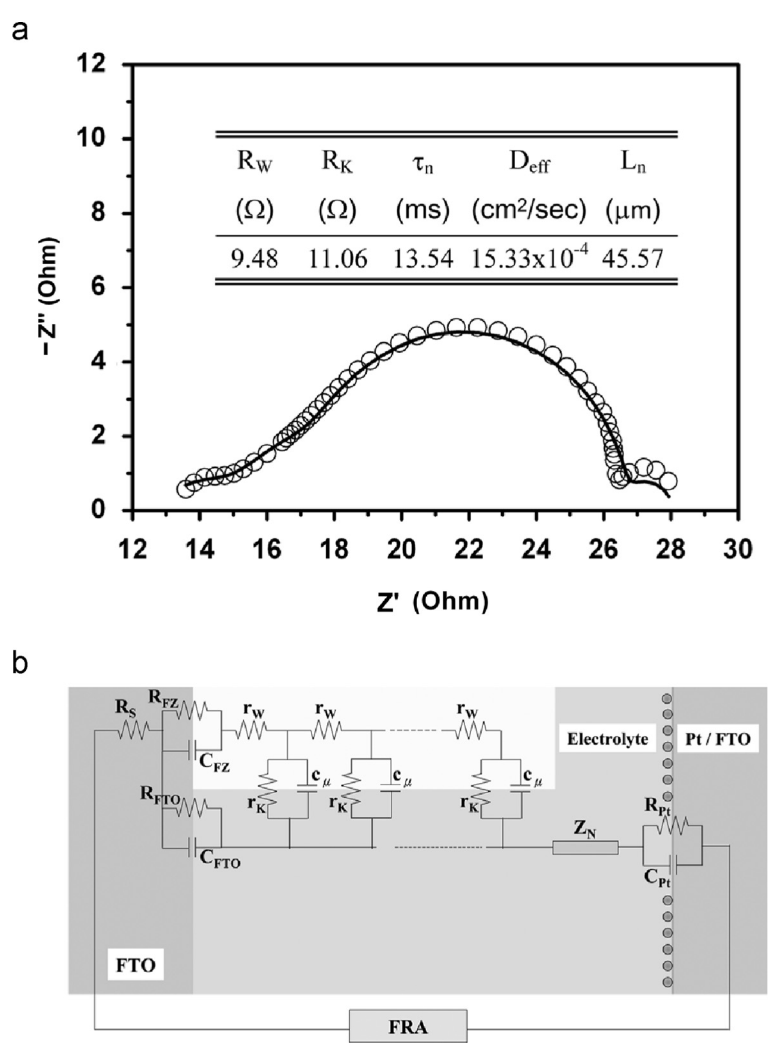


Fig. 6. Nyquist plot of the 42.2 tetrapod-like DSSC. The empty circles in (a) are the measurement data point, and the solid curve is the fitting result based on the equivalent circuit model as shown in (b) [37].

100 kHz) due to the charge transfer at the counter electrode, intermediate frequency region (1 Hz to 1 kHz) due to the ZnO/dye/electrode interface and low frequency region (0.2 Hz to 0.75 Hz) attributed to the diffusion in the redox electrolyte [19,20,57]. The spectra have a peak position or middle frequency peak at 25 Hz (or ω_{max}=25 Hz). The relationship of ω_{max} between τ_{eff} and k_{eff} are

summarized as [17]:

$$\omega_{\max} = k_{eff} = \frac{1}{\tau_{eff}} \tag{9}$$

where k_{eff} represents an effective rate constant for recombination of the electron. The electron lifetime inside the porous ZnO photoanode can be calculated by using Eq. (10). The value of D_{eff} and L_n can be calculated accordingly by using Eqs. (11) and (12) , respectively [17,20,58].

$$\tau_{eff} = \frac{1}{\omega_{ct}} = \frac{1}{2\pi f_{\max}} \tag{10}$$

$$D_{eff} = \frac{R_{ct}\, L^2}{R_t\, \tau_{eff}} \tag{11}$$

$$L_n = L\sqrt{\frac{R_{ct}}{R_t}} \tag{12}$$

On the other hand, the spectra can further be analyzed and fitted by a transmission line equivalent circuit model. Thus, we can obtain the exact value of the electron transport parameters such as τ_{eff}, D_{eff} and L_n. A few equivalent circuit models have been proposed by previous studies of Bisquert, Fabregat-Santiago et al., Wang et al., Fabregat-Santiago et al., Martinson et al., Liberatore et al., Goncalves et al. and Omar et al. to fit the impedance data. Fig. 5 shows a proposed transmission line equivalent circuit model of ZnO and ZnO-CNTs based DSSC that has been published in [39].

At the low frequency region of the impedance spectra (as in Fig. 4), a parallel combination of electron chemical capacitance, C_μ, with charge-transfer resistance, R_{ct}, appeared along the metal oxide semiconductor layer. The diffusion effect by redox species, Z_D also forms as a small spectra/Nyqusit at the lowest frequencies. Sometimes the spectra not appears at all. In addition, the diffusion of electrons in the photoanode layer can be monitored at high frequencies as a Warburg impedance. The spectrum was analyzed belongs to the diffusion resistance, R_t, and chemical capacitance, C_μ at the counter electrode/electrolyte interface (injection of electrons in the electrolyte due to reduction of I_3^- ionic species into I^-). The high frequency arc corresponds to the parallel combination of counter electrode charge transfer resistance, R_{Pt} and Helmholtz capacitance, C_{Pt}. The second arc represents the recombination resistance, R_{ct} and chemical capacitance, C_μ at the metal oxide semiconductor layer/electrolyte interface. Finally, the third arc at low frequencies corresponds to the impedance of diffusion in the electrolyte layer, R_t [19,57]. Consequently, the diameter of arc one, two and three also resembles the R_{Pt}, R_{ct} and R_d (or R_t) element, respectively, while R_s belongs to the initial displacement of the spectra from the origin. In general, the model represents the diffusion of electrons inside the photoanode layer and the recombination effect in the electrolyte interface. Moreover, the equivalent circuit model consists of R_{Pt} and C_{Pt} due to the charge-transfer resistance and capacitance at the counter electrode/electrolyte interface, R_{ct} is the charge-transfer resistance due to the recombination of electrons at photoanode/dye/electrolyte interface, C_μ is the chemical capacitance of the electrode, R_t is the electron transport resistance from the photoanode, R_s is the sheet resistance of the transparent conducting oxide (TCO) glass and geometry of the cell, Z_D is the finite Warburg impedance or diffusion of the redox species in the electrolyte, R_{FTO} and C_{FTO} are the charge-transfer resistance and interfacial capacitance due to electron recombination and charge accumulation at the FTO/electrolyte interface [39]. Thus, a fitting process estimates various electron transport parameters within the ZnO-based DSSC. A few examples are highlighted considering the basic electron transport parameters studied from the TiO_2-based DSSCs. The parameters are listed in Table 1 as analyzed by electrochemical impedance spectroscopy (EIS) unit.

Chiu et al. implemented the EIS analysis to analyze the electron transport inside the photoanode, electrolyte and platinum counter electrode. Fig. 6 shows a Nyquist plot (or impedance spectra) and equivalent circuit model for the tetrapod-like ZnO-based DSSC sensitized with D149 dye [37]. The cell parameters, such as the charge-transfer recombination resistance (R_K), steady-state transport resistance (R_W), electron lifetime (τ_n), effective electron diffusion coefficient (D_{eff}) and film thickness (L_n), have been measured accordingly. Their photovoltaic properties were greatly affected by the thickness of the tetrapod-like ZnO photoanode. The optimized thickness of 42.2 μm with power conversion efficiency, η=4.9% D_{eff}=1.533 × 10^{-3} $cm^2\ s^{-1}$ and L_n=46 μm were estimated

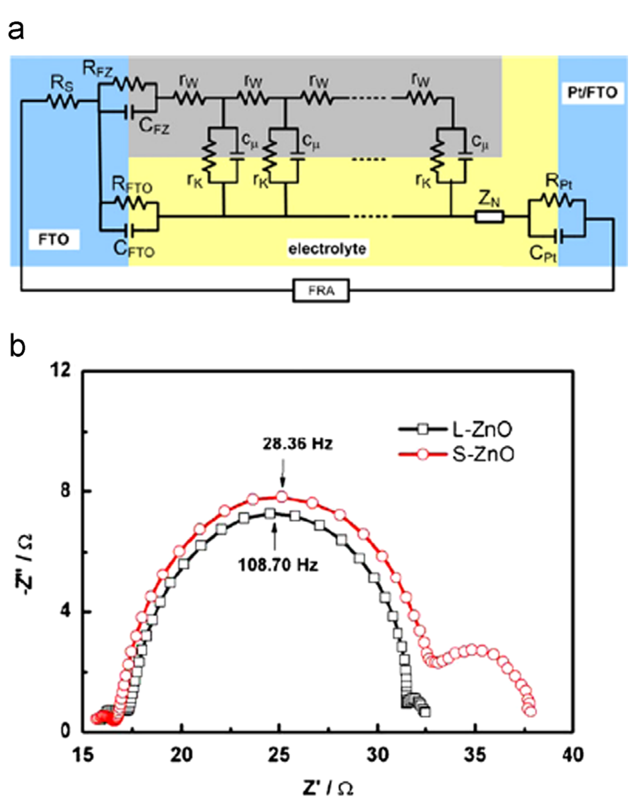


Fig. 7. (a) Equivalent circuit model of short- and long-arms-tetrapod-like ZnO prepared by dc plasma technology (b) Nyquist plot for fitting of the electron transport parameters [59].

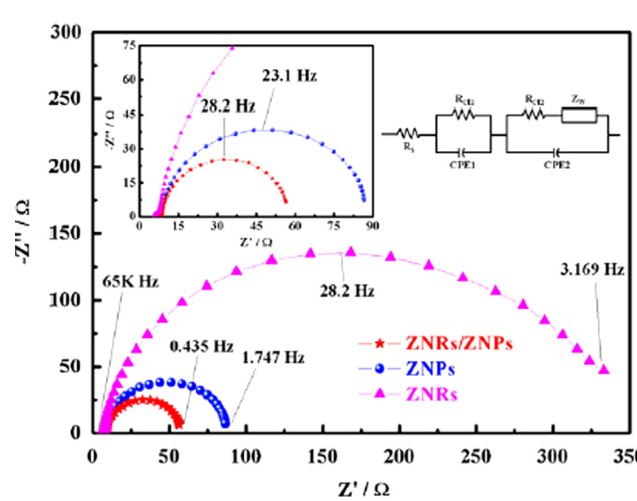


Fig. 8. Electrochemical impedance spectra of the DSSCs with ZNRs, ZNPs and ZNRs/ZNPs [61].

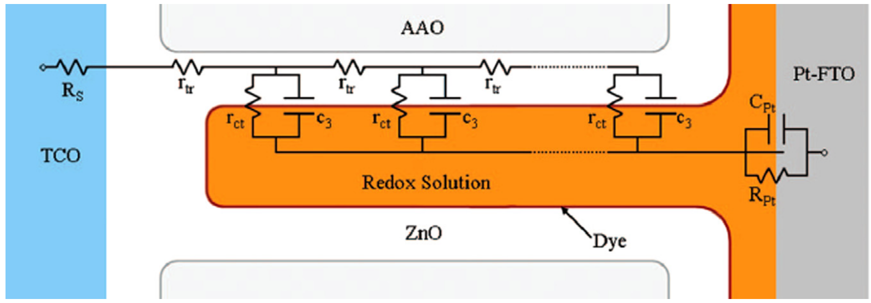


Fig. 9. Equivalent circuit where the impedance spectra are fitted as idealized photoanode schematic [23].

from the EIS unit [37]. He et al. also observed the electron transport and recombination inside the ZnO nanorod-based DSSCs by EIS unit. The Warburg feature of electron transport in the nanorod structures was detected in a high frequency region (Fig. 7). Meanwhile, a constant illumination source reduced the charge transfer resistance, R_{ct} (from 10 kΩ to 200 Ω) and increased the transport resistance, R_t (from 67 Ω to 100 Ω). Theoretically, R_t and R_{ct} should be low and high, respectively. However, in this case, the values of R_t and R_{ct} were found as no dependence upon the illumination effect. They even did not highlighted the relationship between electron transport parameters and photovoltaic performance [59]. Moreover, Lee et al. reported short (S)- and long (L)-arms of tetrapod-like ZnO where S-tetrapod structure shows good photovoltaic performance [60]. The power conversion efficiency, η of 4.78% was measured with $J_{sc}=10.79$ mA cm^{-2}, $V_{oc}=0.66$ V and $FF=0.67$ (Table 1). Consequently, the impedance spectra analysis estimated the peak frequency, ω_{max} at 28.36 Hz with longer electron lifetime, $\tau_{eff}=35.26$ ms but low diffusion coefficient, $D_{eff}=2.47\times10^{-3}$ cm^2 s^{-1} compared to the L-tetrapod-like ZnO. Low D_{eff} was found as a factor that hinders the solar cell performance.

Furthermore, Lin et al. fitted a very simple equivalent circuit or Randle's circuit to fit the electron transport parameters (as in Fig. 8). Their work focused on fabricating three different ZnO nanostructures such as nanorods (NRs), nanoparticles (NPs) and a combination of NRs/NPs. ZnO NRs-based DSSC generated very low power conversion efficiency, η of 0.90%. A composition of ZnO NRs/NPs achieved the highest η of 2.19%. NRs was reported provide 1-D electron transfer pathways between the NPs layer and the substrate. The structures also enhance the light harvesting efficiency compared to the ZnO NRs-based DSSC [61]. Although the electron lifetime of NRs ($\tau_{eff}=2.93$ ms) was estimated as longer than the electron lifetime of NRs/NPs ($\tau_{eff}=1.71$ ms), greater R_{ct} has inhibited the electron transfer into photoanode layer. Table 1 lists the R_{ct} value of NRs, NPs and NRs/NPs. However, the fitting process did not estimate the D_{eff} and L_n. In addition, Martinson et al. also proposed a very simple equivalent circuit model of ZnO-based DSSC without considering the Z_D element (refer to Fig. 9) [23]. The analysis measured very high diffusion of electron in the photoanode layer, $D_{eff}=0.4$ cm^2 s^{-1} which is greater than any ZnO DSSC photoanodes presented in the current report. However, this effect did not influence the power conversion efficiency or total photocurrent density of the cell. The traps inside the photoanode has limited the electron movement and not reached the Fermi level. They even categorized the analysis as a preliminary work and still need further improvement in measuring the D_{eff}. Consequently, a recent report by Omar et al. showed very short electron lifetime, $\tau_{eff}=0.266$ ms and short L_n compared to the photoanode thickness ($L_n \ll L$) [39]. Higher value of R_t compared to R_{ct} also influenced the electron recombination effect inside the cell where R_t was measured about three times greater than R_{ct} ($R_{ct} \ll R_t$). The higher recombination effect has reduced the diffusion of electron into the photoanode layer; $D_{eff}=0.0755\times10^{-3}$ cm^2 s^{-1}. It is very important to obtain higher R_{ct} where it allows the carriers to be accumulated in the capacitive element or chemical capacitance, C_μ of the cell. Bisquert et al. reported C_μ is also associated with the rise of the Fermi level of the photoanode [62]. In this case, the estimation of C_μ was about 7.099 μF as presented in Table 1.The amount of R_{ct} and C_μ greatly influenced the output power of the solar cell where low R_{ct} and C_μ reduced the power conversion efficiency, η to 0.25%.

5. Conclusion

In summary, the unique properties of ZnO photoanode and ease of fabrication make this material applicable for various applications. However, the future of ZnO-based DSSC still depends on increasing the power conversion efficiency by boosting the light harvesting efficiency inside the solar cell, suggesting new materials to develop the photoanode, dye sensitizer, electrolyte and monitoring the energy loss in the cell due to the charge recombination effect, electron trapping and optical reflection [63]. Moreover, suggesting a core-shell structure of ZnO with TiO_2 [64] or a combination of ZnO with carbon nanotubes (CNTs) [65] or graphene [66] are other alternatives to gain better efficiency. However, there is still a challenge to fabricate the hybrid structures as a suitable photoanode with high porosity and good surface structure. From the author's point of view, investigating the electron diffusion inside the cell and reducing the transport resistance, R_t provide a good alternative to investigate the performance of ZnO photoanode. Although, the analysis of electron transport properties and impedance spectra of DSSC was highly focused on reducing the recombination resistance, R_{ct}, the recombination effect is unavoidable in the DSSC's mechanism. In addition, R_{ct} is also known as an intrinsic component of the photophysical process where its influence the solar cell's performance. Nevertheless, a strong recombination must be avoided to make sure the solar cell is not in a failure state due to no injection of electrons into the metal-oxide semiconductor. Moreover, reducing the surface recombination is also a critical factor in generating high power conversion efficiency [62].

Acknowledgements

This work is supported by Photonic Technology Laboratory, IMEN, Department of Electrical, Electronic & Systems, Universiti Kebangsaan Malaysia, Bangi.

References

[1] Chaar LE, lamont LA, Zein NE. Review of photovoltaic technologies. Renewable Sustainable Energy Rev 2011;15:2165–75.
[2] Lee J-J, Rahman MM, Sarker S, Nath NCD, Ahammad AJS, Lee JK. Metal oxides and the composites for the photoelectrode of dye sensitized solar cells. In:

Attaf B, editor. Advances in composite materials for medicine and nanotechnology. Croatia: InTech; 2011. p. 182–210.
[3] Kashyout AB, Soliman M, Gamal ME, M. Fathy M. Preparation and characterization of nano particles ZnO films for dye-sensitized solar cells. Mater Chem Phys 2005;90:230–3.
[4] Chu JB, Huang SM, Zhang DW, Bian ZQ, Li XD, Sun Z, et al. Nanostructured ZnO thin films by chemical bath deposition in basic aqueous ammonia solutions for photovoltaic applications. Appl Phys A 2009;95:849–55.
[5] Villanueva-Cab J, Oskam G, Anta JA. A simple numerical model for the charge transport and recombination properties of dye-sensitized solar cells: a comparison of transport-limited and transfer-limited recombination. Sol Energy Mater Sol Cells 2010;94:45–50.
[6] Grätzel M. Review: dye-sensitized solar cells. J Photochem Photobiol C: Photochem Rev 2003;4:145–53.
[7] Nakamura Y. Solution growth of zinc oxide nanowires for dye-sensitized solar cells. Mat REU Res Accomplishments 2006:74–5.
[8] Nazeeruddin MK, Baranoff E, Grätzel M. Dye-sensitized solar cells: a brief overview. Solar Energy 2011;85:1172–8.
[9] Martinson ABF, Hamann TW, Pellin MJ, Hupp JT. New architectures for dye-sensitized solar cells. Chem A Eur J 2008;14:4458–67.
[10] Grätzel M. Conversion of sunlight to electric power by nanocrystalline dye-sensitized solar cells. J Photochem Photobiol A: Chem 2004;164:3–14.
[11] Halme J. Dye-sensitized nanostructured and organic photovoltaic cells: technical review and preliminary tests. Master's thesis. Helsinki University of Technology; 2002.
[12] Koide N, Islam A, Chiba Y, Han L. Improvement of efficiency of dye-sensitized solar cells based on analysis of equivalent circuit. J Photochem Photobiol A, Chem 2006;182 (296-05).
[13] Han L, Islam A, Chen H, Malapaka C, Chiranjeevi B, Zhang S, et al. High-efficiency dye-sensitized solar cell with a novel co-adsorbent. Energy Environ Sci 2012;5:6057–60.
[14] Burschka J, Pellet N, Moon SJ, Humphry-Baker R, Gao , Nazeeruddin MK, et al. Sequential deposition as a route to high-performance perovskite-sensitized solar cells. Nature 2013;499:316–9.
[15] Goncalves AS, Goes MS, Fabregat-Santiago F, Moehl T, Davolos MR, Bisquert J, et al. Doping saturation in dye-sensitized solar cells based on ZnO:Ga nanostructured photoanodes. Electrochim Acta, 56; 2011; 6503–9.
[16] Fabregat-Santiago F, Bisquert J, Garcia-Belmonte G, Boschloo G, Hagfeldt A. Influence of electrolyte in transport and recombination in dye-sensitized solar cells studied by impedance spectroscopy. Solar Energy Mater Solar Cells 2005;87:117–31.
[17] Bisquert J. Theory of the impedance of electron diffusion and recombination in a thin layer. J Phys Chem B 2002;106:325–33.
[18] Pitarch Á, Garcia-Belmonte G, Mora-Seró I, Bisquert J. Electrochemical impedance spectra for the complete equivalent circuit of diffusion and reaction under steady-state recombination current. J Phys Chem 2004;6:2983–8.
[19] Adachi M, Sakamoto M, Jiu J, Ogata Y, Isoda S. Determination of parameters of electron transport in dye-sensitized solar cells using electrochemical impedance spectroscopy. J Phys Chem B 2006;110:13872–80.
[20] Ariyanto NP, Abdullah H, Syarif J, Yuliarto B, Shaari S. Fabrication of zinc oxide-based dye-sensitized solar cell by chemical bath deposition. Funct Mater Lett 2010;3:303–7.
[21] Bisquert J, Mora-Seró I. Simulation of steady-state characteristics of dye-sensitized solar cells and the interpretation of the diffusion length. J Phys Chem Lett 2010;1:450–6.
[22] Fabregat-Santiago F, Bisquert J, Palomares E, Otero L, Kuang D, Zakeeruddin SM, et al. Correlation between photovoltaic performance and impedance spectroscopy of dye-sensitized solar cells based on ionic liquids. J Phys Chem C 2007;111:6550–60.
[23] Martinson ABF, Góes MS, Fabregat-Santiago F, Bisquert J, Pellin MJ, Hupp JT. Electron transport in dye-sensitized solar cells based on ZnO nanotubes: evidence for highly efficient charge collection and exceptionally rapid dynamics. J Phys Chem 2009;113:4015–21.
[24] Wang Q, Ito S, Grätzel M, Fabregat-Santiago F, Mora-Seró I, Bisquert J, et al. Characteristics of high efficiency dye-sensitized solar cells. J Phys Chem B 2006;110:25210–21.
[25] Liberatore M, Decker F, Burtone L, Zardetto V, Brown TM, Reale A, et al. Using EIS for diagnosis of dye-sensitized solar cells performance. J Appl Electrochem 2009;39:2291–5.
[26] Andrade L, Sousa J, Ribeiro HA, Mendes A. Phenomenological modelling of dye-sensitized solar cells under transient conditions. Solar Energy 2011;85:781–93.
[27] Vasile O-R, Andronescu E, Ghitulica C, Vasile BS, Oprea O, Vasile E, et al. Synthesis and characterization of nanostructured zinc oxide particles synthesized by the pyrosol method. J Nanopart Res 2012;14:1269–81.
[28] Zeng X, Gan YX. Nanocomposites for photovoltaic energy conversion. In: Attaf B, editor. Advances in composite materials for medicine and nanotechnology. Croatia: InTech; 2011. p. 211–66.
[29] Shakti N, Gupta PS. Structural and optical properties of sol–gel prepared ZnO thin film. Appl Phys Res 2010;2:19–28.
[30] Samadi M, Shivaee HA, Zanetti M, Pourjavadi A, Moshfegh A. Visible light photocatalytic activity of novel MWCNT-doped ZnO electrospun nanofibers. J Mol Catal A: Chem 2012;359:42–8.
[31] Patil SL, Chougule MA, Pawar SG, Raut BT, Sen S, Patil VB. New process for synthesis of ZnO thin films: microstructural, optical and electrical characterization. J Alloys Compd 2011;509:10055–61.
[32] Akhavan O, Azimirad R, Safa S. Functionalized carbon nanotubes in ZnO thin films for photoinactivation of bacteria. Mater Chem Phys 2011;130 (598-02).
[33] Baviskar PK, Zhang JB, Gupta V, Chand S, Sankapal BR. Nanobeads of zinc oxide with rhodamine B dye as a sensitizer for dye-sensitized solar cell application. J Alloys Compd 2012;510:33–7.
[34] Peng D, Chen X, Wang Y, Hu Z, Yu K, Zhu Z. Temperature dependent photoluminescence properties of needle-like ZnO nanostructures deposited on carbon nanotubes. Appl Phys A 2011;105:463–8.
[35] Zhu LP, Liao GH, Huang WY, Ma LL, Yang Y, Yu Y, et al. Preparation, characterization and photocatalytic properties of ZnO-coated multi-walled carbon nanotubes. Mater Sci Eng B 2009;163:194–8.
[36] Ilican S, Caglar Y, Caglar M. Preparation and characterization of ZnO thin films deposited by sol–gel spin coating method. J Optoelectr Adv Mater 2008;10: 2578–83.
[37] Chiu W-H, Lee C-H, Cheng H-M, Lin H-F, Liao S-C, Wu J-M, et al. Efficient electron transport in tetrapod-like ZnO metal-free dye-sensitized solar cells. Energy Environ Sci 2009;2:694–8.
[38] Karst N, Rey G, Doisneau B, Roussel H, Deshayes R, Consonni V, et al. Fabrication and characterization of a composite ZnO semiconductor as electron transporting layer in dye-sensitized solar cells. Mater Sci Eng B 2011;176:653–9.
[39] Omar A, Abdullah H, Shaari S, Taha MR. Morphological and electron transport studies in ZnO dye-sensitized solar cell incorporating multi- and single-walled carbon nanotubes. J Phys D: Appl Phys 2013;46:165503.
[40] Lu L, Li R, Peng T, Fan K, Dai K. Effects of rare earth ion modifications on the photoelectrochemical properties of ZnO-based dye-sensitized solar cell. Renewable Energy 2011;36:3386–93.
[41] Martinson ABF. Charge dynamics in new architectures for dye-sensitized solar cells. PhD dissertation. Northwestern University; 2008.
[42] Liu Z, Li Y, Liu C, Ya J, Zhao W, Lei E, et al. Performance of ZnO dye-sensitized solar cells with various nanostructures as anodes. Solid State Sci 2011;13: 1354–9.
[43] Abdullah H, Ariyanto NP, Shaari S, Yuliarto B, Junaidi S. Study of porous nanoflake ZnO for dye-sensitized solar cell application. Am J Eng Appl Sci 2009;2:236–40.
[44] Shishiyanu S, Chow L, Lupan O, Shishiyanu T. Synthesis and characterization of functional nanostructured zinc oxide thin films. Electrochem Soc Trans 2006;3:65–71.
[45] Wahab R, Ansari SG, Kim YS, Seo HK, Kim GS, Khang G, et al. Low temperature solution synthesis and characterization of ZnO nano-flowers. Mater Res Bull 2007;42:1640–8.
[46] Umar A. Growth of comb-like ZnO nanostructures for dye-sensitized solar cells application. Nanoscale Res Lett 2009;4:1004–8.
[47] Kakiuchi K, Hosono E, Kimura T, Imai H, Fujihara S. Fabrication of mesoporous ZnO nanosheets from precursor templates grown in aqueous solution. J Sol–Gel Sci Technol 2006;39:63–72.
[48] Cheng HM, Chiu WH, Lee CH, Tsai SY, Hsieh WF. Formation of branched ZnO nanowires from solvothermal method and dye-sensitized solar cells applications. J Phys Chem 2008;112:16359–64.
[49] Ariyanto NP, Abdullah H, Shaari S, Junaidi S, Yuliarto B. Preparation and characterization of porous nanosheets zinc oxide film: based on chemical bath deposition. World Appl Sci J 2009;6:764–8.
[50] Keis K, Magnusson E, Lindström H, Lindquist S, Hagfeldt AA. 5% efficient photoelectrochemical solar cell based on nanostructured ZnO electrodes. Solar Energy Mater Solar Cells 2002;73:51–8.
[51] Hossain MF, Takahashi T, Biswas S. Nanorods and nanolipsticks structured ZnO photoelectrode for dye-sensitized solar cells. Electrochem Comm 2009;11: 1756–9.
[52] Keis K, Bauer C, Boschloo G, Hagfeldt A, Westermark K, Rensmo H, et al. Nanostructured ZnO electrodes for dye-sensitized solar cell applications. J Photochem Photobiol A: Chem 2002;148:57–64.
[53] Choopun S, Tubtimtae A, Santhaveesuk T, Nilphai S, Wongrat E, Hongsith N. Zinc oxide nanostructures for applications as ethanol sensors and dye-sensitized solar cells. Appl Surf Sci 2009;256 (998-02).
[54] Grätzel M, Durrant JR. Dye-sensitized mesoscopic solar cells. In: Archer MD, Nozik AJ, editors. Nanostructured and photoelectrochemical systems for solar photon conversion. London: Imperial College Press; 2008. p. 503–36.
[55] Ahmed S. Beneficial microstructured TiO_2 photoanodes for improving DSSC performance. PhD dissertation. The State University of New Jersey; 2011.
[56] Kern R, Sastrawan R, Ferber J, Stangl R, Luther J. Modeling and interpretation of electrical impedance spectra of dye solar cells operated under open-circuit conditions. Electrochem Acta 2002;47:4213–25.
[57] Wang Q, Moser JE, Grätzel M. Electrochemical impedance spectroscopic analysis of dye-sensitized solar cells. J Phys Chem B 2005;109:14945–53.
[58] Ariyanto NP. Study on synthesis of mesoporous zinc oxide film as photoanode towards performance of dye-sensitized solar cell. Master thesis. University Kebangsaan Malaysia; 2011.
[59] He C, Zheng Z, Tang H, Zhao L, Lu F. Electrochemical impedance spectroscopy characterization of electron transport and recombination in ZnO nanorod dye-sensitized solar cells. J Phys Chem C 2009;113:10322–5.
[60] Lee C-H, Chiu W-H, Lee K-M, Yen W-H, Lin H-F, Hsieh W-F, et al. The influence of tetrapod-like ZnO morphology and electrolytes on energy conversion efficiency of dye-sensitized solar cells. Electrochim Acta 2010;55:8422–9.
[61] Lin L-Y, Yeh M-H, Lee C-P, Chou C-Y, Vittal R, Ho K-C. Enhanced performance of a flexible dye-sensitized solar cell with a composite semiconductor film of ZnO nanorods and ZnO nanoparticles. Electrochim Acta 2012;62:341–7.

[62] Bisquert J, Fabregat-Santiago F. Impedance spectroscopy: a general introduction and application to dye-sensitized solar cells. In: Kalyanasundaram K, editor. Dye-sensitized solar cells. Switzerland: CRC Press; 2010. p. 457–554.
[63] Zhang Q, Cao G. Nanostructured photoelectrodes for dye-sensitized solar cells. Nano Today 2011;6:91–109.
[64] Zhang Q, Dandeneau CS, Zhou X, Cao G. ZnO Nanostructures for dye-sensitized solar cells. Adv Mater 2009;21:4087–108.
[65] Zeng G-Y, Nian K-S, Lee K-Y. Characteristics of a dye-sensitized solar cell based on an anode combining ZnO nanostructures with vertically aligned carbon nanotubes. Diam Relat Mater 2010;19:1457–60.
[66] Fang X, Li M, Guo K, Zhu Y, Hu Z, Liu X, et al. Improved properties of dye-sensitized solar cells by incorporation of graphene into the photoelectrodes. Electrochim Acta 2012;65:174–8.